10. IEEE_TIA_A_Dual_Five-Phase_Space-Vector_Modulation_Algorithm_Based_on_the_Decomposition_Method[1]

by Metta Savitri

Submission date: 13-Apr-2023 08:04AM (UTC-0500)
Submission ID: 2063427803
File name: or_Modulation_Algorithm_Based_on_the_Decomposition_Method_1.pdf (1.62M)
Word count: 7000
Character count: 36421

A Dual Five-Phase Space-Vector Modulation Algorithm Based on the Decomposition Method

Martin Jones, I. Nyoman Wahyu Satiawan, Nandor Bodo, *Student Member, IEEE*, and Emil Levi, *Fellow, IEEE*

***Abstract*—Open-end winding variable speed drives with dual-inverter supply have been extensively investigated for various applications, including series hybrid power-trains and propulsion motors. The topology is simple to realize while offering a higher number of switching states without the need for capacitor voltage balancing algorithms, when compared to standard multilevel converters. The overwhelming majority of work is, however, restricted to the three-phase electric machinery. One of the reasons for this is that inclusion of a multiphase machine leads to exponential increase in the number of possible switching states, and so the design of a suitable space vector modulator (SVM) represents a considerable challenge. This paper considers a relatively simple SVM algorithm based on the decomposition of the three-level space vector decagon into a number of two-level decagons. The proposed modulation technique has the advantage of being relatively simple to implement. The drive produces multilevel load phase voltages with negligible low-order harmonic content. Despite the simplicity of the method, the quality of the output voltages is improved, compared to the previously proposed methods. The developed scheme is verified via detailed simulations and experiments using a five-phase induction machine under open-loop V/f control.**

***Index Terms*—Induction motor drives, multiphase ac drives, open-end winding, space vector modulation.**

I. Introduction

MULTILEVEL and multiphase voltage source inverters (VSIs) have been attracting increasing research interest recently due to their ability to overcome voltage and current limitations of power semiconductors and their inherent ability to tolerate faults [1]–[3]. Multilevel inverters are considered as a topology which enhances the quality of the output voltage waveform, reduces dv/dt, and enables the construction of a high power converter without the problem of switching series-connected semiconductor devices. There are numerous configurations of multilevel converters, the main ones being the neutral point clamped (NPC), the flying capacitor, and the cascaded converters [4].

The open-end winding topology, originally described in [5], can be considered as an alternative approach to create multilevel load phase voltage waveforms. The equivalence of the topology with a two-level inverter on each side of the stator winding and three-level or four-level single-sided supplied drive (depending on the dc-bus voltage ratio) is shown in terms of performance and created multilevel load phase voltages in [6] for three-phase drives. The open-end topology has the advantages that the additional diodes used in the NPC VSI are not needed, leading to a saving in the overall number of components. Furthermore, the issue of proper capacitor voltage balancing does not exist if the supply is two level at each winding side. Typically, three-phase VSIs are utilized. It has been suggested in the literature that such drives may, in the future, offer an alternative supply solution in applications such as EVs/HEVs [7]–[9], electric ship propulsion [10], and rolling mills [11]. Recent research efforts have been directed toward investigating the potential of this supply configuration in renewable electric energy systems [12] and fault-tolerant drives [13].

Due to their well-known advantages [1], multiphase drives have also been considered for similar applications as the multilevel drives. As a consequence, some researchers have begun investigating the benefits of combining both technologies [14]–[24]. Recently, some research effort has been directed toward the multiphase open-end winding topology [14]–[18]. An asymmetrical six-phase induction motor drive has been developed in [14], [15]. In [14], the supply is provided by means of two isolated two-level six-phase VSIs. The goal was in essence low-order harmonic elimination/reduction rather than the multilevel operation, so that the dual converter is not operated in multilevel mode. The topology discussed in [15] uses four three-phase two-level inverters, with four isolated dc sources, to prevent circulation of zero sequence currents. The space vector modulator (SVM) control is performed in essence independently for the two three-phase windings, using the nearest three vectors approach in conjunction with three-level inverter. The work is focused on controlling the power sharing between the four converters. The five-phase configuration has been examined in [16], [17] and a suitable SVM algorithm proposed. In [18], the SVM algorithm of [17] is extended to the seven-phase structure.

The remaining literature is primarily centered on the five-phase NPC VSI fed drive [19]–[23]. The first SVM techniques for multiphase VSIs were based on the simple extension of the three-phase multilevel SVM approaches, so that only the three vectors, nearest to the reference, were utilized [19]. As a consequence, only the first plane of the multiphase system is controlled. In principle, the number of applied vectors must equal the number of phases [1]. Hence, numerous low-order harmonics are generated, which map into the second plane. A

Manuscript received December 30, 2011; revised March 20, 2012; accepted April 1, 2012. Date of publication October 25, 2012; date of current version December 31, 2012. Paper 2011-IPCC-795.R1, approved for publication in the IEEE TRANSACTIONS ON INDUSTRY APPLICATIONS by the Industrial Power Converter Committee of the IEEE Industry Applications Society. This work was supported by NPRP Grant 4-152-02-053 from the Qatar National Research Fund (a member of the Qatar Foundation). The statements made herein are solely the responsibility of the authors.

The authors are with the School of Engineering, Technology and Maritime Operations, Liverpool John Moores University, Liverpool, L3 3AF, U.K. (e-mail: M.Jones2@ljmu.ac.uk; I.N.Satiawan@2008.ljmu.ac.uk; N.bodo@2009.ljmu.ac.uk; e.levi@ljmu.ac.uk).

Color versions of one or more of the figures in this paper are available online at http://ieeexplore.ieee.org.

Digital Object Identifier 10.1109/TIA.2012.2226422

SVM method, which controls both planes, has been developed in [20] for the three-level NPC VSI fed five-phase drive, and it was extended to the seven-phase case in [21]. The SVM method is complicated, particularly the sector identification, since each 36° sector is partitioned into ten subsectors. A different approach to the SVM of multilevel multiphase systems is given for a general case of an m-level, n-phase VSI in [22]. The algorithm is based on the considerations of the multidimensional (n-dimensional) space and therefore does not include decomposition of the n-dimensional space into 2-D planes. A somewhat similar method, in the sense that decomposition into 2-D planes is not utilized, is the one in [23], where a multiphase multilevel PWM is developed using n single-leg modulators. Level-shifted and phase-shifted carrier-based PWM methods have recently been applied to the five-phase open-end topology in [24], where it was shown that PWM methods developed for NPC converters can be applied to the five-phase open-end topology.

This paper develops further the modulation method originally proposed in [25] for a five-phase open-end winding drive, based on two two-level inverters. The SVM algorithm is based on the decomposition of the three-level space vector decagon into a number of two-level decagons. A similar idea has been proposed in [26] for a three-phase NPC inverter and in [27] for a three-phase open-end winding drive. In the case of the five-phase open-end winding drive, the situation is significantly more complicated since both 2-D planes have to be considered. It is shown here that the algorithm proposed in [26] can lead to an increase in the dc-link voltage of one of the inverters, over a small operating range, and a simple solution is suggested as a remedy. The proposed modulation strategy is verified for the first time using detailed simulations and a set of experiments. The results indicate that the method is capable of achieving the target fundamental while eliminating fully any low-order harmonic content in the output load phase voltage. Furthermore, the modulation method gives superior harmonic performance to the one given in [17].

The paper begins with a review of the five-phase two-level drive characteristics followed by a general description and mathematical model of the cascaded topology, including mapping of the space vectors into the 2-D planes. Next, the proposed modulation method is described. It is shown that due to the nature of the five-phase topology one of the inverters needs to be operated using so-called multi-frequency SVM [28] and the inverters must operate with slightly different dc-link voltages. Finally, simulation and experimental results verify the performance of the drive.

II. General Properties of Two-Level Five-Phase Drives

Prior to considering the SVM scheme for the open-end winding topology, it is beneficial to review the basic relationships which govern the performance of five-phase drives and the corresponding two-level SVM technique for a five-phase VSI. A five-phase machine can be modeled in two 2-D subspaces, so-called $\alpha - \beta$ and $x - y$ subspaces [1]. It can be shown that only current harmonic components which map into the $\alpha - \beta$ subspace develop useful torque and torque ripple, whereas those

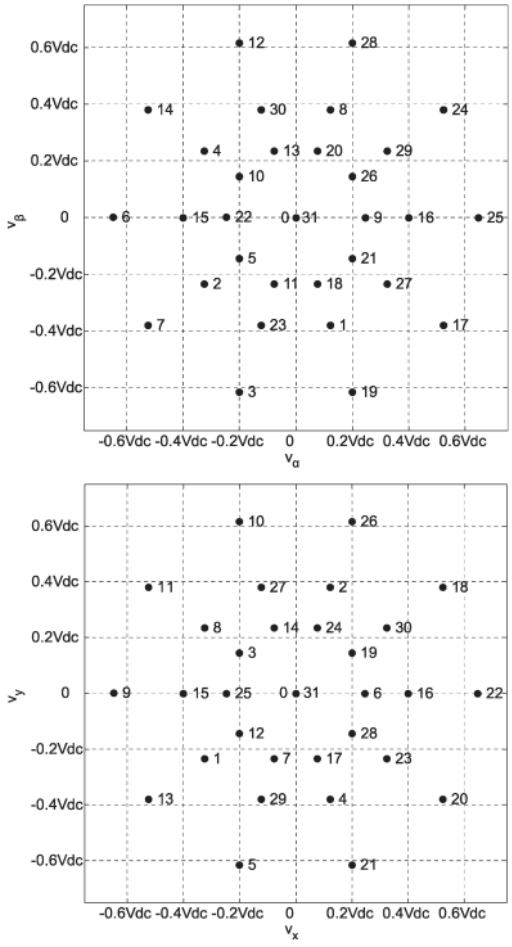

Fig. 1. Two-level five-phase VSI space vectors in the $\alpha - \beta$ and $x - y$ planes.

that map into the $x - y$ subspace do not contribute to the torque at all. A multiphase machine with near-sinusoidal magnetomotive force distribution presents extremely low impedance to all non-flux/torque producing supply harmonics, and it is therefore mandatory that the supply does not generate such harmonics. What this means is that the design of a five-phase PWM strategy must consider simultaneously both 2-D subspaces, where the reference voltage, assuming pure sinusoidal references, is in the first plane while reference in the other plane is zero. Two-level five-phase inverters can generate up to $2^5 = 32$ voltage space vectors with corresponding components in the $\alpha - \beta$ and $x - y$ subspaces, as shown in Fig. 1. Space vectors are labeled with decimal numbers, which, when converted into binary code, reveal the values of the switching functions of each of the inverter legs. Active (non-zero) space vectors belong to three groups in accordance with their magnitudes - small, medium and large space vector groups. The magnitudes are identified with indices s, m, and l and are given as, respectively, $|\underline{v}_s| = 4/5\cos(2\pi/5)V_{\rm dc}$, $|\underline{v}_m| = 2/5V_{\rm dc}$, and $|\underline{v}_l| = 4/5\cos(\pi/5)V_{\rm dc}$. Four active space vectors are required

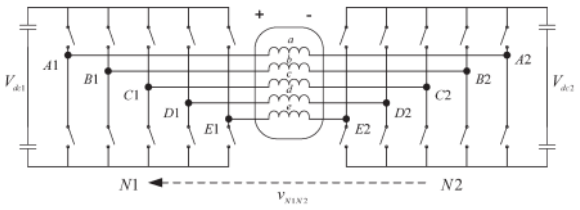

Fig. 2. Five-phase open-end winding topology.

to generate sinusoidal voltages [1]. In order to provide zero average voltage in the $x-y$ plane two neighboring large and two medium space vectors are selected [29]. It is shown in [30], [31] that the maximum peak value of the output fundamental phase-to-neutral voltage in the linear modulation region is $v^{h1\,\max} = 0.525V_{\rm dc}$, resulting in the maximum modulation index, $M = 1.05$. Switching pattern is a symmetrical PWM with two commutations per inverter leg.

III. Five-Phase Open-End Winding Topology

Fig. 2 illustrates the open-end winding structure, based on utilisation of two two-level five-phase VSIs. The two inverters are identified with indices 1 and 2. Inverter legs are denoted with capital letters, A, B, C, D, E and the negative rails of the two dc-links are identified as $N1$ and $N2$. Machine phases are labeled as a, b, c, d, e. Load phase voltage positive direction is with reference to the left inverter (inverter 1). Two isolated dc supplies are assumed so that the common mode voltage (CMV) v_{N1N2} is of non-zero value (the issue of CMV elimination is not addressed here). The resulting space vectors in dual-inverter supply mode will depend on the ratio of the two dc-link voltages. When the dc-link voltages are equal, i.e., $V_{\rm dc1} = V_{\rm dc2} = V_{\rm dc}/2$, the resulting space-vector pattern is identical to the equivalent single-sided three-level supply. Using the notation of Fig. 2, load phase voltages of the stator winding can be given as

$$\begin{aligned} v_a &= v_{A1N1} + v_{N1N2} - v_{A2N2} \\ v_b &= v_{B1N1} + v_{N1N2} - v_{B2N2} \\ v_c &= v_{C1N1} + v_{N1N2} - v_{C2N2} \\ v_d &= v_{D1N1} + v_{N1N2} - v_{D2N2} \\ v_e &= v_{E1N1} + v_{N1N2} - v_{E2N2}. \end{aligned} \tag{1}$$

Space vectors of load phase voltages in the two planes are determined with

$$\begin{aligned} \underline{v}_{\alpha-\beta} &= (2/5)\left(v_a + \underline{a}v_b + \underline{a}^2 v_c + \underline{a}^3 v_d + \underline{a}^4 v_e\right) \\ \underline{v}_{x-y} &= (2/5)\left(v_a + \underline{a}^2 v_b + \underline{a}^4 v_c + \underline{a}^6 v_d + \underline{a}^8 v_e\right) \end{aligned} \tag{2}$$

where $\underline{a} = \exp(j2\pi/5)$. Using (1) and (2), one gets

$$\begin{aligned} \underline{v}_{\alpha-\beta} &= \underline{v}_{\alpha-\beta(A1B1C1D1E1)} - \underline{v}_{\alpha-\beta(A2B2C2D2E2)} \\ \underline{v}_{x-y} &= \underline{v}_{x-y(A1B1C1D1E1)} - \underline{v}_{x-y(A2B2C2D2E2)} \end{aligned} \tag{3}$$

since $v_{N1N2}(1 + \underline{a} + \underline{a}^2 + \underline{a}^3 + \underline{a}^4) = 0$.

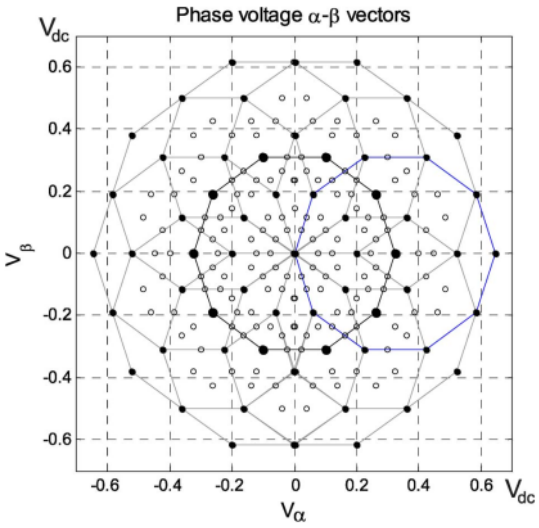

Fig. 3. Space-vector distribution of the dual-inverter supplied five-phase open-end topology in the $\alpha-\beta$ plane, $V_{\rm dc1} = V_{\rm dc2} = V_{\rm dc}/2$.

In (3), the two space vectors on the right-hand sides of the two equations are corresponding voltage space vectors of the two five-phase two-level VSIs, which come in three different lengths already discussed in the previous section. Their combinations result in 211 voltage space vectors, produced by 1024 possible switching states [16].These are illustrated in Fig. 3 for the $\alpha-\beta$ plane. Space-vector mapping into the $x-y$ plane follows the pattern that exists for a five-phase VSI, the largest vectors of the first plane map into the smallest vectors of the second plane and so on. A consequence of the greater number of voltage space vectors is an increased number of load phase voltage levels.

IV. Principle of the Proposed Algorithm

Another consequence of the large number of switching states and space vectors is that the development of a suitable SVM strategy is challenging. The complexity of selecting the proper switching states for a given command voltage can be significantly reduced if the three-level space-vector decagon is decomposed into a number of two-level decagons as shown in Fig. 3. A similar approach was followed in [27] for the three-phase case. The center decagon comprises vectors which can be activated if one inverter is used up to half of the achievable maximum voltage with the other one locked in a zero vector state. As a consequence, the converter is in two-level mode of operation based on four active and zero vector application, as discussed in Section II and [29]. As can be seen in Fig. 3, the origins of the outer decagons are located on the outer vectors of the inner decagon, denoted by the larger dots in Fig. 3, which correspond to the outermost vectors and switching states given in Fig. 1. In the case of the three-phase topology [27], operation in the outer region (outer hexagon) is achieved when one inverter operates with a single voltage space vector applied (the nearest one to the reference), and the second inverter

is modulated using the standard three-phase two-level SVM technique. Let the applied vector for one inverter be $\underline{v}_i$, and let the reference be $\underline{v}^*$. Here, $\underline{v}_i$ is the vector produced by the inverter that is the nearest to the reference, and $\underline{v}^*$ exceeds, in magnitude, maximum voltage realizable with one inverter. The reference for the other inverter is then set as

$$\underline{v}^{**} = -(\underline{v}^* - \underline{v}_i). \tag{4}$$

In other words, when the magnitude of the reference voltage exceeds the maximum value obtainable with one inverter, one inverter is operated in six-step (i.e., ten-step) mode, while the second inverter is modulated in the standard way.

It is well known that operation of a five-phase inverter in ten-step mode, without a controllable dc-link voltage, leads to uncontrollable fundamental output voltage magnitude and unwanted low-order harmonics, which, for the leg voltage of inverter 1, can be expressed as a Fourier series as

$$v_{\text{leg}} = \frac{2}{\pi} V_{\text{dc1}} \left[\sin \omega t + \frac{1}{3} \sin 3\omega t + \frac{1}{5} \sin 5\omega t + \frac{1}{7} \sin 7\omega t \ldots \right]. \tag{5}$$

In a five-phase system, harmonics of the order $10k \pm 1 (k = 0, 1, 2, 3 \ldots)$ map onto the torque/flux producing subspace, $\alpha - \beta$, while harmonics of the order $10k \pm 3$ map into the $x - y$ subspace. They do not produce any useful torque/flux and simply lead to large unwanted loss-producing currents. The large currents are a consequence of the relatively small impedance presented in $x - y$ plane. $10k \pm 5$ are zero-sequence components. This leads to the requirement that the second inverter must be able to not only control the fundamental but also eliminate the unwanted low-order harmonics, which are produced by applying only the large vector in the $\alpha - \beta$ plane from one inverter. This causes unwanted harmonics in both planes since a large vector has a corresponding non-zero value in the second, $x - y$ plane (Fig. 1). In order to achieve this objective, the second inverter modulation scheme will need to operate in both the $\alpha - \beta$ and the $x - y$ planes, since the references for the second inverter can be given as

$$\begin{aligned} v_\alpha^{**} &= -\left(v_\alpha^* - v_{i(\alpha)}\right) \quad v_\beta^{**} = -\left(v_\beta^* - v_{i(\beta)}\right) \\ v_x^{**} &= v_{i(x)} \quad v_y^{**} = v_{i(y)}. \end{aligned} \tag{6}$$

Here, $i = 1 \ldots 10$ stands for the large vector of the first VSI. A SVM, which achieves simultaneous control in both the $\alpha - \beta$ and $x - y$ planes, was developed in [28] in order to control multiphase multi-motor drive systems. A schematic illustration of the SVM process is shown in Fig. 4. This SVM method utilizes two two-level five-phase SVMs, as described in Section II. Each space-vector modulator operates in a separate plane. The duty cycles from the SVMs are summed according to the phase transposition rule [32]. The phase transposition [32] enables the lower five-phase SVM to operate in the $x - y$ plane. This further simplifies the algorithm since identification of the sector, dwell time calculation and the vector look-up table are identical for both modulators.

As a result of the proposed modulation technique for the open-end winding configuration, the converter operates using

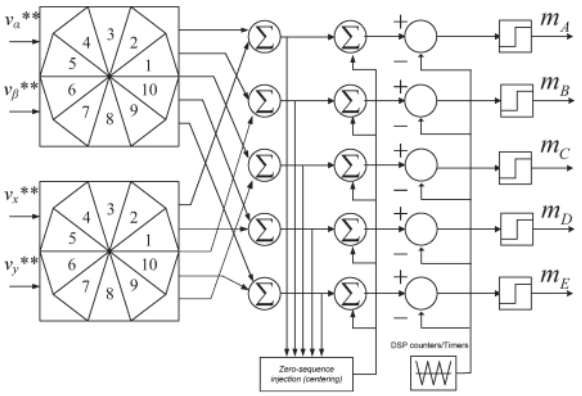

Fig. 4. Signal flow of the five-phase multi-frequency space-vector modulator.

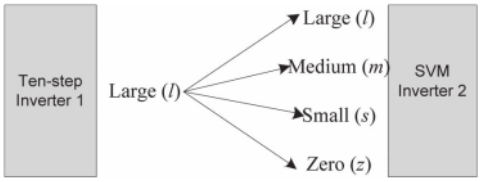

Fig. 5. Five-phase dual-inverter switching combinations.

only the large vectors from one inverter and any combination of vectors from the other inverter, as illustrated in Fig. 5. This reduces the number of switching states to 342 (320 of these are the states met when both inverters operate, while 22 states are those that are encountered when only one inverter operates). The 342 switching states produce 151 vectors in the $\alpha - \beta$ and $x - y$ planes, as shown in Fig. 6. It can be seen that no large vectors are produced in the $x - y$ plane. Taking into account the number of space vectors and (1), the maximum number of load phase voltage levels is 15. A signal flow diagram of the complete space-vector modulation scheme is presented in Fig. 7(a). When $M < 0.525$, the switches in Fig. 7(a) are opened (in the upper position), meaning that the ten-step inverter is locked, with all upper or lower switches on, (i.e., so-called zero vector is applied), thus forming a star connection and the machine is supplied in single-sided mode. The second inverter is operated as a two-level inverter according to the SVM method outlined in Section II and discussed in detail in [29].

It is interesting to note that the two-level multiphase SVM method employs the same space vectors for the same dwell-times as one carrier-based PWM method [29] and thus gives the same results in terms of phase and line-to-line voltages. This equivalent carrier-based PWM method is the one with offset injection (i.e., zero-sequence signal injection), defined as $v_{zs} = -0.5(\max\{v_j^*\} + \min\{v_j^*\}, \; j = a, b, c, d, e$. Therefore, it can be concluded that the multi-frequency two-level modulator of Fig. 4 may be replaced with a carrier-based approach. Such an approach is shown in Fig. 7(b). It follows that the simulation and experimental results presented in this paper for the SVM are equally applicable to the carrier-based two-level modulation method with offset injection.

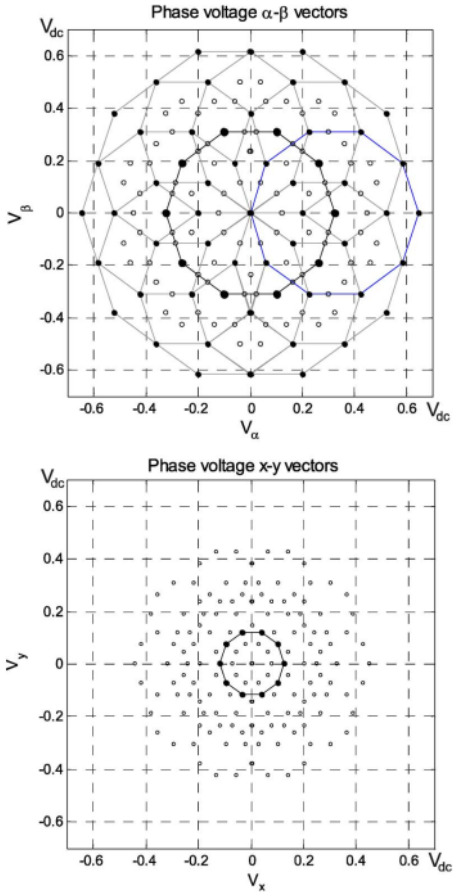

Fig. 6. Decomposed SVM space-vector distribution of the dual-inverter supplied open-end winding five-phase topology, in the $\alpha - \beta$ and $x - y$ planes.

V. DC-Link Voltages

For clarity, it is beneficial to define the modulation index of the space vector-modulated inverter as $M_2 = v^{**}/(0.5V_{\mathrm{dc2}})$. Only inverter 2 is operational up to the point when $M = 0.525(M_2 = 1.05)$. Hence, the converter operates in two-level mode, since inverter 1 is not engaged and is locked in a zero switching state 11111 or 00000, forming a neutral point. It is worth noting that the converter output is still significantly improved compared to the equivalent two-level single-sided configuration since the inverter is switching across the load half of the equivalent two-level converter's dc-link voltage. When $M > 0.525$, the second inverter operates in ten-step mode. In this operating regime, the space vector-modulated inverter will output the difference between the voltages created by the ten-step mode inverter and the reference. Since the output fundamental voltage of the ten-step inverter is fixed, there is a narrow band of modulation indices $(0.525 < M \leq 0.637)$ where the fundamental output voltage of the ten-step inverter is greater than the reference voltage. Therefore, in this operating region, the SVM inverter acts to decrease the fundamental created by the ten-step inverter. At these modulation indices, all the power is supplied by the ten-step inverter, and what is

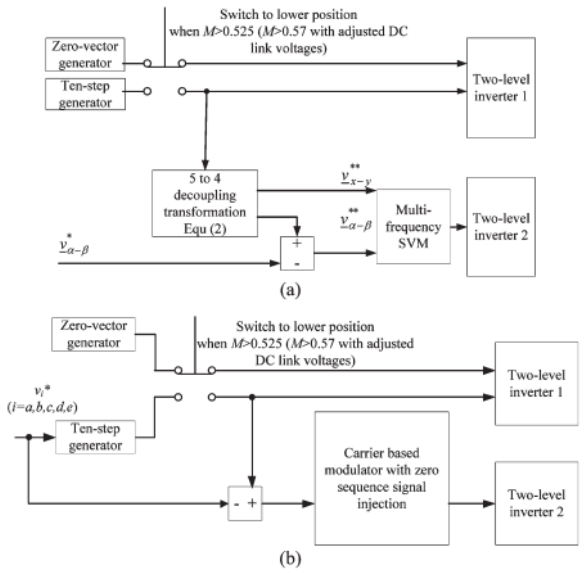

Fig. 7. Signal flow of the decomposition method using SVM modulator (a) or a carrier-based modulator (b).

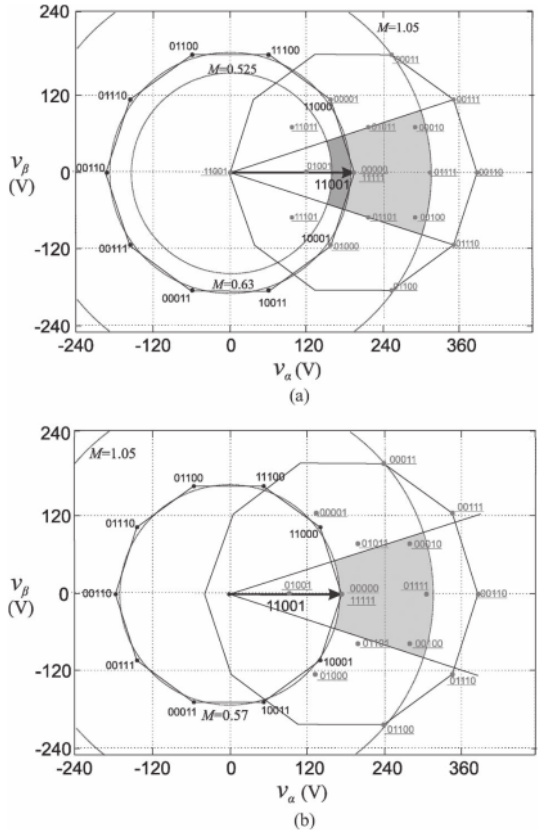

Fig. 8. Operating regions for system with equal 300-V dc-link voltages (a) and adjusted dc-link voltages (b).

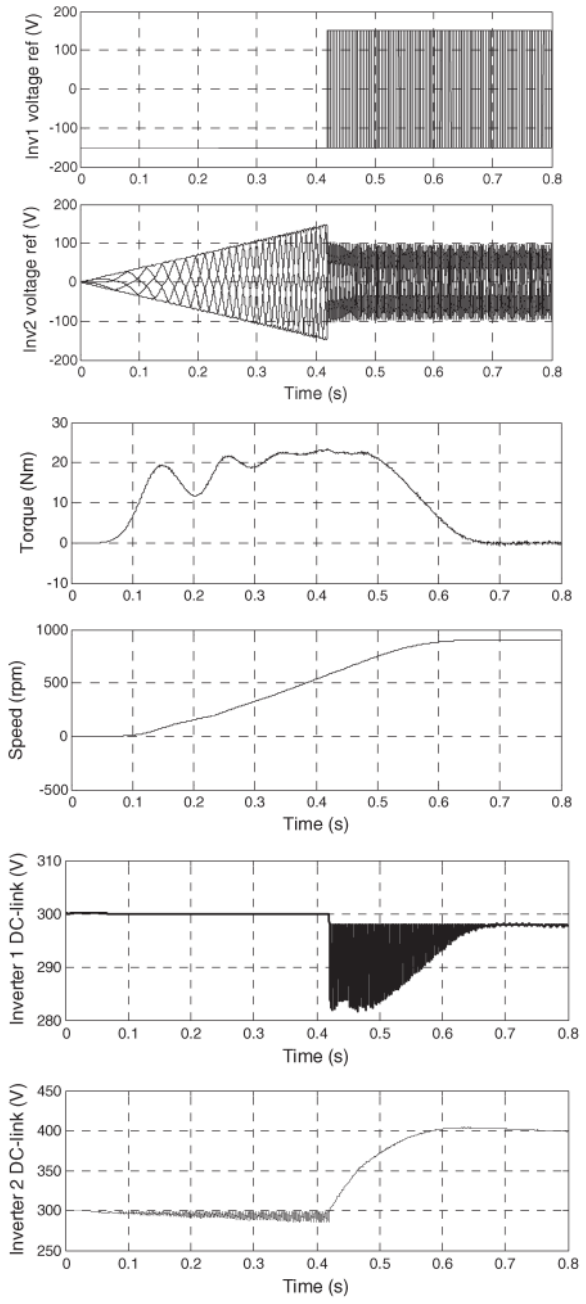

Fig. 9. Acceleration to 30 Hz with equal dc-link voltages: Inverter references, torque, speed response, and inverter dc-link voltages.

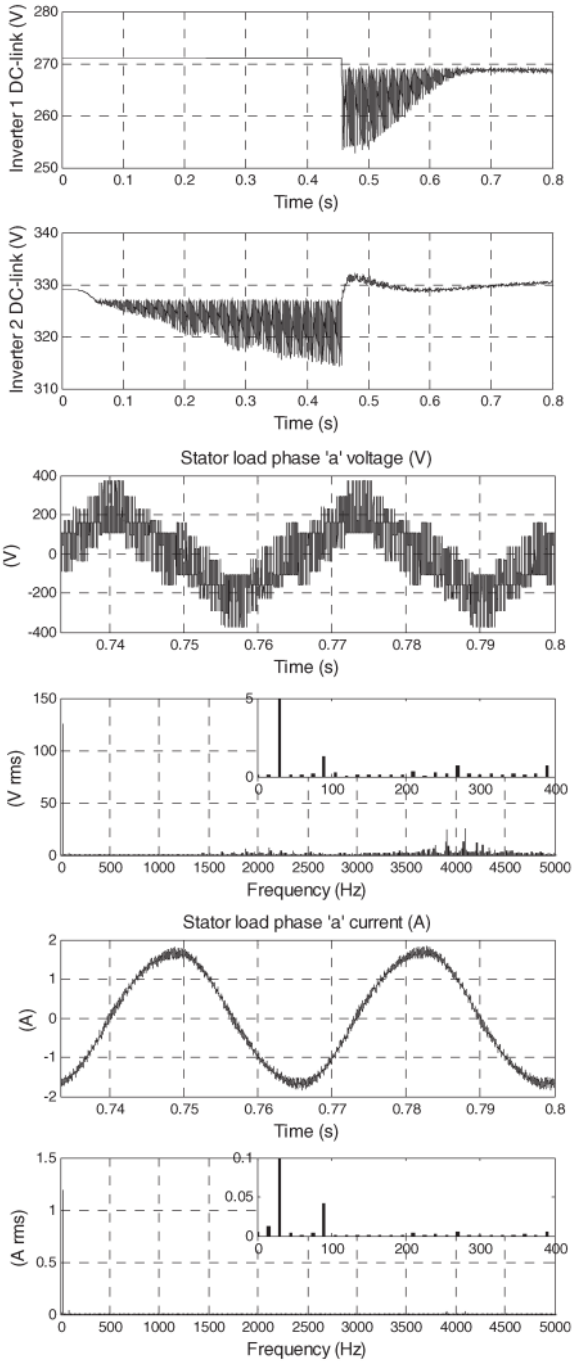

Fig. 10. Acceleration to 30 Hz with adjusted dc-link voltages according to (10) and (11): Inverter dc-link voltages, machine phase "a" voltage and stator phase "a" current waveforms and spectra.

not consumed by the load is absorbed by the SVM inverter. If there is no regenerative rectifier on the side of the SVM inverter, its dc-link capacitor voltage will raise until the braking chopper is activated, and the energy is dissipated. Fig. 8(a) depicts the switching states used when the large vector 11001 is applied by the ten-step inverter along with the reference circular path for the relevant modulation indices. $M = 1.05$ is the maximum modulation index, $M = 0.525$ is half of the maximum modulation index, the point at which the ten-step inverter starts to operate, and the lower boundary where the dc-link voltage increase begins. $M = 0.637$ (i.e., $2/\pi$) coincides with the magnitude of the fundamental of the ten-step inverter and is the upper boundary of dc-link voltage increase after

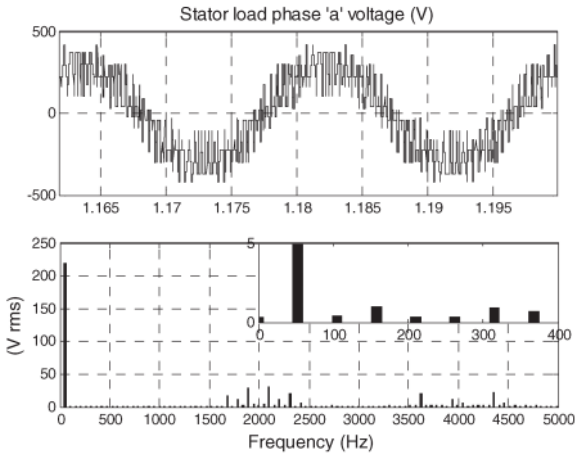

Fig. 11. Operation at $M = 1.05$, with adjusted dc-link voltages: Machine phase "a" voltage waveform and spectrum.

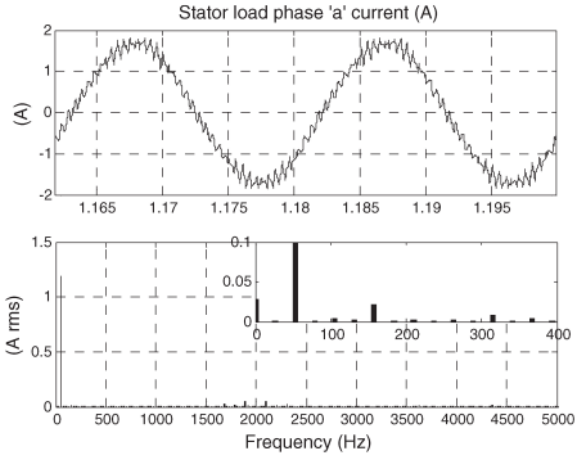

Fig. 12. Operation at $M = 1.05$, with adjusted dc-link voltages: Machine stator phase "a" current waveform and spectrum.

which no further increase is seen. The black dots in Fig. 8 are the vectors applied by the ten-step inverter, while the gray dots with underlined binary numbers are the vectors applied during the operation of both inverters. The increase is strongly dependent on the inductive part of the load impedance and can be substantial, leading to activation of the dynamic brake in the SVM inverter. One way to prevent this issue is to adjust the dc-link voltage ratio in such a way that the first harmonic of the ten-step inverter output equals the fundamental generated by the SVM inverter when at maximal modulation index, when operated on its own

$$v_1^{h1} = v_2^{h1\,\max}. \tag{7}$$

The maximum achievable fundamental for a five-phase two-level SVM inverter is given with [29]

$$v_2^{h1\,\max} = \frac{V_{\mathrm{dc2}}}{2\cos(\pi/10)}. \tag{8}$$

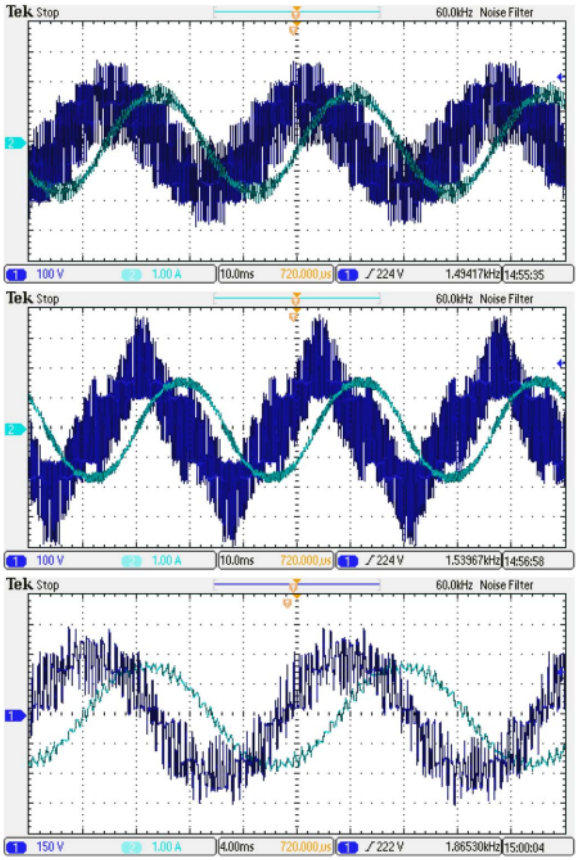

Fig. 13. Oscilloscope recordings of load phase voltage and current waveforms at $M = 0.55$ (top), $M = 0.6$ (middle), and $M = 1.05$ (bottom).

The fundamental voltage of the ten-step inverter is from (5)

$$v_1^{h1} = \frac{2}{\pi} V_{\mathrm{dc1}} \tag{9}$$

Setting $V_{\mathrm{dc}} = V_{\mathrm{dc1}} + V_{\mathrm{dc2}} = 600$ V to give the equivalent of single-sided three-level supply with a 600-V dc-link and taking into account (7)–(9), the required values for the individual inverter dc-link voltages are:

$$V_{\mathrm{dc1}} = \frac{600}{1 + 4\cos\left(\frac{\pi}{10}\right)/\pi} = 271.38\ \mathrm{V} \tag{10}$$

$$V_{\mathrm{dc2}} = \frac{600}{1 + \pi/4\cos\left(\frac{\pi}{10}\right)} = 328.62\ \mathrm{V}. \tag{11}$$

The highest achievable peak fundamental of the SVM inverter is

$$v_2^{h1\,\max} = v_1^{h1} = \frac{600}{2\cos\left(\frac{\pi}{10}\right) + \pi/2} = 172.76\ \mathrm{V} \tag{12}$$

which corresponds to the modulation index $M = 0.57$. This means that the SVM inverter will operate alone up to $M = 0.57 (M_2 = 1.05)$.When $M > 0.57$ the ten-step inverter will operate as well. The adjustment of the dc-link voltages obviously leads to a somewhat different layout of the space

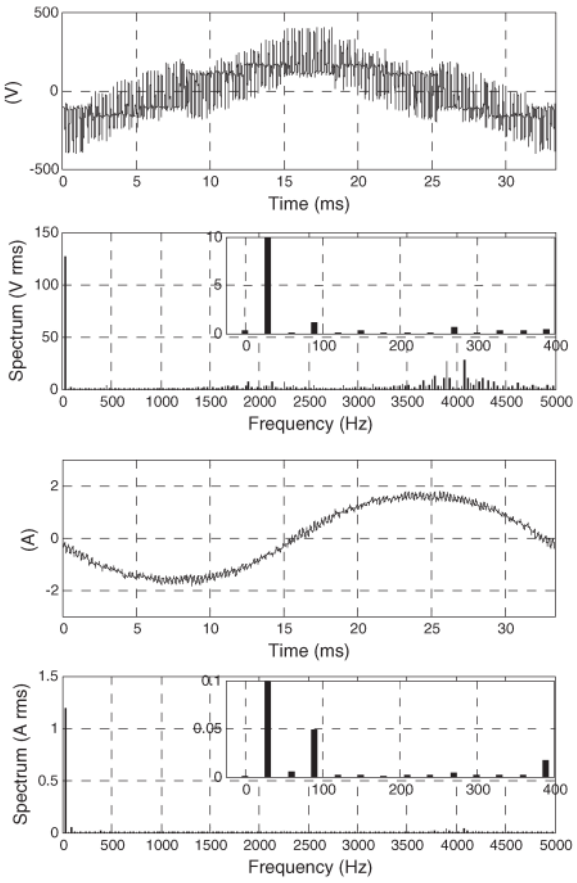

Fig. 14. Load phase voltage (top) and current (bottom) waveforms and spectra at $M = 0.6$.

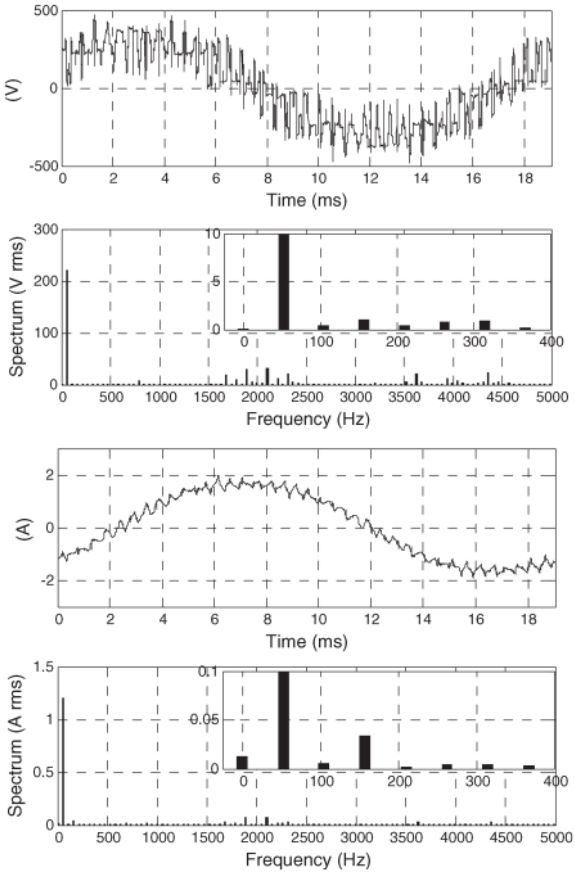

Fig. 15. Load phase voltage (top) and current (bottom) waveforms and spectra at $M = 1.05$.

vectors of the open-end winding converter, as shown in Fig. 8(b) for the case when the ten-step inverter applies the vector 11001. It can be seen that, although the SVM inverter applies the same switching states as in Fig. 8(a), the operating regions have changed, and the small region where the SVM inverter dc-link voltage is boosted has disappeared.

VI. Simulation Verification

In order to verify the converter's performance, a series of detailed simulations were undertaken using the PLECS environment. Initially, the dc-link voltage of each inverter is 300 V ($V_{\mathrm{dc1}} = V_{\mathrm{dc2}} = V_{\mathrm{dc}}/2$), the switching frequency of the modulated inverter is 2 kHz, and the implemented dead time is 6 μs. The IGBT and diode models include an on-state resistance of 10 mΩ. The drive is operated in open-loop V/f mode. The voltage reference profile is such that the supply frequency of the machine is ramped from zero to 50 Hz in 0.8 s. At the operating frequency of 50 Hz the modulation index $M = 1$ is reached. Voltage boost is not included. The machine parameters are $L_{\gamma s} = 45$ mH, $L_{\gamma r} = 15$ mH, $L_m = 515$ mH, $R_r = 3\ \Omega$ and $R_s = 3\ \Omega$ and are those of the induction machine used further on in the experiments. First, acceleration of the drive from standstill to 900 rpm (30 Hz) is examined. Fig. 9 shows the developed torque and speed, the dc-link voltages, and the leg voltage references of the inverters. The dc-link voltage of the SVM inverter experiences a considerable increase. It can be seen that the increase coincides with the activation of the ten-step inverter (inverter 1) and is therefore a consequence of the excessive fundamental provided by the ten-step inverter.

Next, the individual inverter dc-link voltages are adjusted according to (10) and (11), and the simulation is re-run. The inverter references and machine torque response are similar to those already presented and are hence not given. Fig. 10 shows the dc-link voltage of the inverters, the steady-state machine phase "a" voltage and current waveforms and spectra. Clearly, the adjusted dc-link voltage setting has prevented the rise in dc-link voltage. The load phase voltage shows the converter operating in multilevel mode. The voltage and current spectra show a small amount of low-order harmonic content, predominantly the third. It is shown in [33], [34] that these harmonics are a consequence of the dead time and can be eliminated by a suitable closed-loop current control method. In other words, the low-order harmonics are not a direct result of the modulation method. Figs. 11 and 12 present the stator phase "a" voltage and current waveforms and spectra, respectively, for the case when

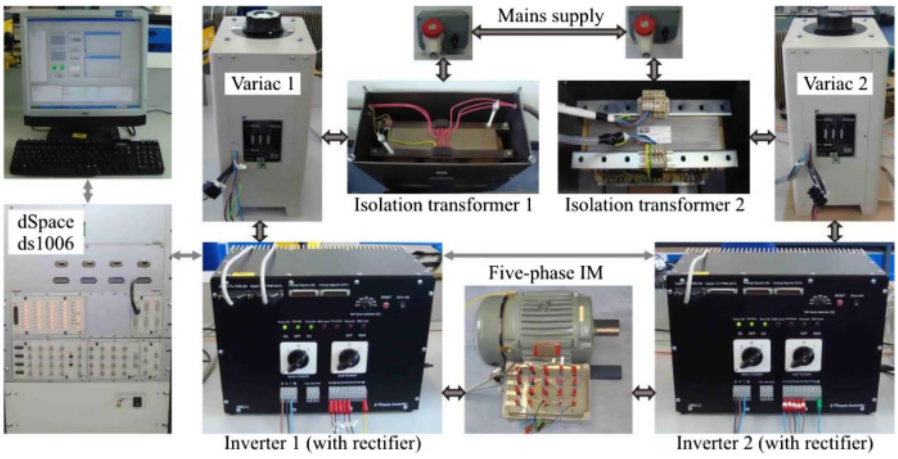

Fig. 16. Experimental setup.

$M = 1.05$ (maximum). The load phase voltage and current contain again a small amount of low-order harmonics and the fundamental magnitude matches the reference.

VII. Experimental Verification

The experimental results are obtained using two custom built five-phase two-level VSIs which utilize Infineon's FS50R12KE3 IGBTs. A four-pole five-phase induction motor is connected to the converter. Each stator phase consists of two half-windings, which can be connected in series or in parallel. In this paper, the half-windings are series connected. Parameters of this motor have been used in the simulation study of Section VII. The inverters are controlled using a dSPACE DS1006 processor board. The dSPACE module is connected to the VSIs via a dSPACE DS5101 digital waveform unit. The dc-link voltages are created for the two inverters of the open-end topology by using two isolation transformers, to isolate the mains supply, and variacs to adjust the voltage according to (10) and (11). The switching frequency of the SVM inverter is 2 kHz, and the inverter dead time is 6 μs. The motor is controlled in open-loop V/f mode with the maximum modulation index ($M = 1.05$) being reached when the fundamental frequency is 52.5 Hz.

The waveforms are obtained using a Tektronix MSO 2014 Mixed Signal Oscilloscope. The machine phase "a" voltage is obtained using a Tektronix P5205A High Voltage Differential Probe, while the current waveform on channel 2 is obtained using a Tektronix TCP0030 Current Probe. Oscilloscope screen shots, showing the machine phase "a" voltage and current, are presented in Fig. 13 for operation when $M = 0.55$, $M = 0.6$ and $M = 1.05$. It can be seen that the converter operates in two-level mode when $M = 0.55$, as evidenced by the nine levels in the load phase voltage. When $M = 0.6$, the ten-step inverter is operational, and the converter operates in multilevel mode. Operation at $M = 1.05$ produces the maximum number of load phase voltage levels.

Figs. 14 and 15 depict the voltage and current waveforms and their associated spectra for the case when $M = 0.6$ and $M = 1.05$, respectively. The FFTs of the load phase voltage and currents are obtained by measuring the load phase voltages and currents in 125 000 points. The resolution of the waveforms obtained in this way enables processing by Matlab to calculate the spectra. A good agreement between simulations and experiments can be observed by comparing Figs. 10–12 with Figs. 14 and 15. The voltage and current waveforms and FFTs match reasonably well. A small amount of low-order harmonics appears in the simulation and experimental results, and the rms of the fundamental reaches the expected level. Inevitably, there are some very minor disagreements, caused by un-modeled phenomena and imprecise parameters such as semiconductor turn-on and turn-off times, voltage drops on the semiconductors, machine parameters, and stray capacitances.

A photograph of the experimental setup is given in Fig. 16.

VIII. Conclusion

This paper has presented a SVM method for the dual-inverter five-phase open-end winding topology. The algorithm is relatively easy to implement since the modulation of the multilevel converter is considered from the perspective of two five-phase two-level converters. It is shown in the paper that the dc-link voltages of the individual converters must be properly selected in order to avoid unwanted power transfer from one dc-link to the other dc-link, which may cause an unacceptable rise of the dc-link voltage of one inverter. When the modulation index is below the value of 0.57, the converter operates in two-level mode utilizing a single inverter. When the reference fundamental exceeds the capabilities of a single inverter (that is, the modulation index is more than 0.57), one inverter operates in ten-step mode, and the other is multi-frequency space vector modulated. As a result, the converter is operated in multilevel mode. The multi-frequency modulated inverter is used to add the required value to the fundamental voltage and eliminate any low-order harmonics created by the ten-step mode inverter. The method has been verified by simulation and experimental investigation.

REFERENCES

[1] E. Levi, "Multiphase electric machines for variable-speed applications," *IEEE Trans. Ind. Electron.*, vol. 55, no. 5, pp. 1893–1909, May 2008.

[2] P. Lezana, J. Pou, T. A. Meynard, J. Rodriguez, S. Ceballos, and F. Richardeau, "Survey on fault operation on multilevel inverters," *IEEE Trans. Ind. Electron.*, vol. 57, no. 7, pp. 2207–2218, Jul. 2010.

[3] S. Kouro, M. Malinowski, K. Gopakumar, J. Pou, L. G. Franquelo, B. Wu, J. Rodriguez, M. A. Perez, and J. I. Leon, "Recent advances and industrial applications of multilevel converters," *IEEE Trans. Ind. Electron.*, vol. 57, no. 8, pp. 2553–2580, Aug. 2010.

[4] P. W. Hammond, "A new approach to enhance power quality for medium voltage drives," in *Proc. IEEE Ind. Appl. Soc. 42nd Annu. Petroleum Chem. Ind. Conf.*, Denver, CO, 1995, pp. 231–235.

[5] H. Stemmler and P. Guggenbach, "Configurations of high-power voltage source inverter drives," in *Proc. EPE Appl. Conf*, Brighton, U.K., 1993, vol. 5, pp. 7–14.

[6] K. A. Corzine, S. D. Sudhoff, and C. A. Whitcomb, "Performance characteristics of a cascaded two-level converter," *IEEE Trans. Energy Convers.*, vol. 14, no. 3, pp. 433–439, Sep. 1999.

[7] B. A. Welchko and J. M. Nagashima, "A comparative evaluation of motor drive topologies for low-voltage, high-power EV/HEV propulsion systems," in *Proc. IEEE ISIE*, Rio de Janerio, Brazil, 2003, pp. 379–384.

[8] C. Rossi, G. Grandi, P. Corbelli, and D. Casadei, "Generation system for series hybrid powertrain based on the dual two-level inverter," presented at the EPE Appl. Conf., Barcelona, Spain, 2009, 0978.

[9] G. Grandi, C. Rossi, A. Lega, and D. Casadei, "Multilevel operation of a dual two-level inverter with power balancing capability," in *Conf. Rec. IEEE IAS Annu. Meeting*, Tampa, FL, 2006, pp. 603–610.

[10] L. Shuai and K. Corzine, "Multilevel multiphase propulsion drives," in *Proc. IEEE Electric Ship Technologies Symposium ESTS*, Philadelphia, PA, 2005, pp. 363–370.

[11] Y. Kawabata, M. Nasu, T. Nomoto, E. C. Ejiogu, and T. Kawabata, "High-efficiency and low acoustic noise drive system using open-winding AC motor and two space-vector-modulated inverters," *IEEE Trans. Ind. Electron.*, vol. 49, no. 4, pp. 783–789, Aug. 2002.

[12] G. Grandi, C. Rossi, D. Ostojic, and D. Casadei, "A new multilevel conversion structure for grid-connected PV applications," *IEEE Trans. Ind. Electron.*, vol. 56, no. 11, pp. 4416–4426, Nov. 2009.

[13] Y. Wang, T. A. Lipo, and D. Pan, "Robust operation of double-output AC machine drive," in *Proc. IEEE ICPE ECCE Asia*, Jeju, Korea, 2011, pp. 140–144.

[14] K. K. Mohapatra and K. Gopakumar, "A novel split phase induction motor drive without harmonic filters and with linear voltage control for the full modulation range," *Eur. Power Electron. J.*, vol. 16, no. 4, pp. 20–28, 2006.

[15] G. Grandi, A. Tani, P. Sanjeevikumar, and D. Ostojic, "Multiphase multilevel AC motor drive based on four three-phase two-level inverters," in *Proc. Int. SPEEDAM*, Pisa, Italy, 2010, pp. 1768–1775.

[16] E. Levi, M. Jones, and W. Satiawan, "A multiphase dual-inverter supplied drive structure for electric and hybrid electric vehicles," presented at the IEEE VPPC, Lille, France, 2010, 95-45630.

[17] E. Levi, I. N. Satiawan, N. Bodo, and M. Jones, "A space-vector modulation scheme for multilevel open-end winding five-phase drives," *IEEE Trans. Energy Convers.*, vol. 27, no. 1, pp. 1–10, Mar. 2012.

[18] N. Bodo, M. Jones, and E. Levi, "Multilevel space-vector PWM algorithm for seven-phase open-end winding drives," in *Proc. IEEE ISIE*, Gdansk, Poland, 2011, pp. 1881–1886.

[19] C. M. Hutson, G. K. Venayagamoorthy, and K. A. Corzine, "Optimal SVM switching for a multilevel multiphase machine using modified discrete PSO," presented at the IEEE SIS, St. Louis, MO, 2008, 4 668 326.

[20] L. Gao and J. E. Fletcher, "A space vector switching strategy for three-level five-phase inverter drives," *IEEE Trans. Ind. Electron.*, vol. 57, no. 7, pp. 2332–2343, Jul. 2010.

[21] O. Dordevic, M. Jones, and E. Levi, "A space-vector PWM algorithm for a three-level seven-phase voltage source inverter," presented at the EPE Appl. Conf., Birmingham, U.K., 2011, 0123.

[22] O. López, J. Alvarez, J. Doval-Gandoy, and F. D. Freijedo, "Multilevel multiphase space vector PWM algorithm with switching state redundancy," *IEEE Trans. Ind. Electron.*, vol. 56, no. 3, pp. 792–804, Mar. 2009.

[23] J. I. Leon, S. Vaquez, J. A. Sanchez, R. Portillo, L. G. Franquelo, J. M. Carrasco, and E. Dominguez, "Conventional space-vector modulation techniques versus the single-phase modulator for multilevel converters," *IEEE Trans. Ind. Electron.*, vol. 57, no. 7, pp. 2473–2482, Jul. 2010.

[24] N. Bodo, E. Levi, and M. Jones, "Carrier-based modulation techniques for five-phase open-end winding drive topology," in *Proc. IEEE IECON*, Melbourne, Australia, 2011, pp. 3656–3661.

[25] M. Jones, I. N. Satiawan, and E. Levi, "A three-level five-phase space-vector modulation algorithm based on the decomposition method," in *Proc. IEEE IEMDC*, Niagara Falls, ON, Canada, 2011, pp. 1219–1224.

[26] A. K. Gupta and A. M. Khambadkone, "A space vector PWM scheme for multilevel inverters based on two-level space vector PWM," *IEEE Trans. Ind. Electron.*, vol. 53, no. 5, pp. 1631–1639, Oct. 2006.

[27] G. Shiny and M. R. Baiju, "Space Vector PWM scheme without sector identification for an open-end winding induction motor based 3-level inverter," in *Proc. IEEE IECON*, Porto, Portugal, 2009, pp. 1310–1315.

[28] D. Dujic, G. Grandi, M. Jones, and E. Levi, "A space vector PWM scheme for multifrequency output voltage generation with multiphase voltage-source inverters," *IEEE Trans. Ind. Electron.*, vol. 55, no. 5, pp. 1943–1955, May 2008.

[29] D. Dujic, M. Jones, and E. Levi, "Continuous carrier-based vs. space vector PWM for five-phase VSI," in *Proc. IEEE EUROCON*, Warsaw, Poland, 2007, pp. 1772–1779.

[30] A. Iqbal, E. Levi, M. Jones, and S. N. Vukosavic, "Generalised sinusoidal PWM with harmonic injection for multiphase VSIs," in *Proc. IEEE PESC*, Jeju, Korea, 2006, pp. 2871–2877.

[31] E. Levi, D. Dujic, M. Jones, and G. Grandi, "Analytical determination of dc-bus utilization limits in multiphase VSI supplied AC drives," *IEEE Trans. Energy Convers.*, vol. 23, no. 2, pp. 433–443, Jun. 2008.

[32] E. Levi, M. Jones, S. N. Vukosavic, and H. A. Toliyat, "A novel concept of a multiphase, multi-motor vector controlled drive system supplied from a single voltage source inverter," *IEEE Trans. Power Electron.*, vol. 19, no. 2, pp. 320–335, Mar. 2004.

[33] M. Jones, D. Dujic, E. Levi, and S. N. Vukosavic, "Dead-time effects in voltage source inverter fed multiphase AC motor drives and their compensation," presented at the EPE Appl. Conf., Barcelona, Spain, 2009, 0001.

[34] M. Jones, S. N. Vukosavic, D. Dujic, and E. Levi, "A synchronous current control scheme for multiphase induction motor drives," *IEEE Trans. Energy Convers.*, vol. 24, no. 4, pp. 860–868, Dec. 2009.

Martin Jones received the B.Eng. degree (First Class Honors) in electrical engineering from Liverpool John Moores University, Liverpool, U.K., in 2001. He was a research student at Liverpool John Moores University from September 2001 until Spring 2005, when he received the Ph.D. degree. Mr Jones was a recipient of the IEE Robinson Research Scholarship for his Ph.D. studies.

He is currently a Reader at Liverpool John Moores University. His research is in the area of high-performance ac drives.

I. Nyoman Wahyu Satiawan was born in Singaraja, Bali, Indonesia, in 1970. He received the first degree in electrical engineering from the University of Udayana, Bali, Indonesia, in 1996, and the M.Sc. degree in control engineering and the Ph.D. degree from Liverpool John Moores University, Liverpool, U.K., in 2001 and 2012, respectively.

He joined the University of Mataram, West Nusa Tenggara, Indonesia, as an academic in 1998. His research interests are in the area of electric motor drives and power converters.

Nandor Bodo (S'11) received the Master's degree in power electronics from the University of Novi Sad, Novi Sad, Serbia, in 2009. Currently, he is working toward the Ph.D. degree at Liverpool John Moores University, Liverpool, U.K.

His research interests include power electronics and variable-speed drives.

Emil Levi (S'89–M'92–SM'99–F'09) received the M.Sc. and Ph.D. degrees from the University of Belgrade, Belgrade, Yugoslavia, in 1986 and 1990, respectively.

From 1982 until 1992, he was with the Department of Electrical Engineering, University of Novi Sad. He joined Liverpool John Moores University, Liverpool, U.K., in May 1992 and has been, since September 2000, a Professor of Electric Machines and Drives.

Prof. Levi serves as an Editor of the IEEE TRANSACTIONS ON ENERGY CONVERSION, a Co-Editor-in-Chief of the IEEE TRANSACTIONS ON INDUSTRIAL ELECTRONICS, and as the Editor-in-Chief of the *IET Electric Power Applications*. He was the recipient of the Cyril Veinott Award of the IEEE Power and Energy Society for 2009 and the Best Paper Award of the IEEE TRANSACTIONS ON INDUSTRIAL ELECTRONICS for 2008.

10. IEEE_TIA_A_Dual_Five-Phase_Space-Vector_Modulation_Algorithm_Based_on_the_Decompositio...

ORIGINALITY REPORT

17%	10%	15%	2%
SIMILARITY INDEX	INTERNET SOURCES	PUBLICATIONS	STUDENT PAPERS

MATCH ALL SOURCES (ONLY SELECTED SOURCE PRINTED)

1%

★ Dujic, Drazen, Martin Jones, Emil Levi, Joel Prieto, and Federico Barrero. "Switching Ripple Characteristics of Space Vector PWM Schemes for Five-Phase Two-Level Voltage Source Inverters—Part 1: Flux Harmonic Distortion Factors", IEEE Transactions on Industrial Electronics, 2011.

Publication

Exclude quotes	On	Exclude matches	Off
Exclude bibliography	On		

10. IEEE_TIA_A_Dual_Five-Phase_Space-Vector_Modulation_Algorithm_Based_on_the_Decomposition_M

GRADEMARK REPORT

FINAL GRADE

/0

GENERAL COMMENTS

Instructor

PAGE 1

PAGE 2

PAGE 3

PAGE 4

PAGE 5

PAGE 6

PAGE 7

PAGE 8

PAGE 9

PAGE 10

PAGE 11